

Prediction of matrix crack initiation and evolution and their effect on the stiffness of laminates with off-axis plies under in-plane loading

Socci, Carlo Alberto; Kassapoglou, Christos

DOI

[10.1016/j.compscitech.2020.108427](https://doi.org/10.1016/j.compscitech.2020.108427)

Publication date

2020

Document Version

Final published version

Published in

Composites Science and Technology

Citation (APA)

Socci, C. A., & Kassapoglou, C. (2020). Prediction of matrix crack initiation and evolution and their effect on the stiffness of laminates with off-axis plies under in-plane loading. *Composites Science and Technology*, 200, Article 108427. <https://doi.org/10.1016/j.compscitech.2020.108427>

Important note

To cite this publication, please use the final published version (if applicable). Please check the document version above.

Copyright

Other than for strictly personal use, it is not permitted to download, forward or distribute the text or part of it, without the consent of the author(s) and/or copyright holder(s), unless the work is under an open content license such as Creative Commons.

Takedown policy

Please contact us and provide details if you believe this document breaches copyrights. We will remove access to the work immediately and investigate your claim.



Prediction of matrix crack initiation and evolution and their effect on the stiffness of laminates with off-axis plies under in-plane loading

Carlo Alberto Socci, Christos Kassapoglou*

Chair of Aerospace Structures and Computational Mechanics, Department of Aerospace Engineering, Delft University of Technology, Delft, Netherlands

ARTICLE INFO

Keywords:

B: Matrix cracking
Stiffness degradation
B: Non-linear behaviour
B: Plastic deformation
A: Laminate

ABSTRACT

A model is described which allows the exact calculation of stresses in a cracked ply under combined state of strain. Closed form expressions for the stresses in each ply are combined in an energy density-based criterion to predict crack spacing and the resulting transverse modulus and shear modulus. Inelastic effects due to non-linearities of the ply-level shear stress-strain curve are accounted for through computation of the permanent shear strain in the ply. The model accounts for ply thickness, stacking sequence and load redistribution effects of a relatively broad class of laminates. Comparisons with test results for a variety of laminates and materials show very good to excellent agreement. The approach developed is extremely efficient and can easily be incorporated in numerical progressive failure analysis, where the stiffness properties of each element can be updated every time the crack pattern changes and in fatigue analysis where the stiffness of a ply or a laminate can be determined during every load cycle.

1. Introduction

Given that damage will occur during the life of a composite structure, it is important to predict its effect on structural performance. This requires accurate calculation of basic properties such as stiffness and strength. In broad terms, damage in composite laminates takes the form of matrix cracking, fiber fractures and delaminations. Of these, matrix cracking can occur at relatively low loads, well within a structure's "design envelope" [1]. Matrix cracking can significantly reduce the effective transverse and shear stiffnesses of a ply, which, in turn, can cause degradation of the laminate's overall stiffness and Poisson's ratio [2,3].

Highsmith and Reifsnider [4] were among the first who worked on rigorously modeling stiffness degradation due to matrix cracking in off-axis plies. Through a 1D shear lag analysis, the deformation of cracked plies was tied to matrix crack density. Agreement with experimental results was good for cross-ply laminates under uniaxial tension. Laws, Dvorak and Hejazi [1,5] followed by modeling the cracked ply material as a two-phase medium where the stiffness matrix of a ply was expressed as a function of matrix crack density. However, as Hashin pointed out [6], this approach does not account accurately for the constraints imposed on a matrix crack by adjacent plies. Stiffness degradation due to matrix cracking in cross-ply laminates was also

treated by Hashin [6,7] using a variational approach. He found that, for a cross-ply laminate under uniaxial tension, accounting for cracks in the 0° plies has almost no effect on the longitudinal stiffness, and a strong effect on the major Poisson's ratio. Caslini, Zanotti and O'Brien [2], used a shear lag analysis proposed by Ogin et al. [3] to relate matrix crack density to stiffness degradation. At about the same time, Nuismer and Tan [8] used a simplified shear lag problem to solve for the stresses in a cracked laminate.

Varna, Joffe et al. [9,10] have made considerable contributions in this field. Their work drew on and complemented Talreja's work [11–13], who developed a synergistic approach to damage modeling combining micromechanics with continuum damage mechanics. The models by Varna, Joffe et al. [9,10] give good predictions for the effect of cracks in any off-axis ply but require tests on laminates with 90° plies in every location through the thickness where an off-axis ply is required.

Van Paepegem, De Baere and Degriek modelled the nonlinear shear stress-strain response of GFRP laminates [14,15]. Their approach uses continuum damage mechanics and requires experimental data from the shear stress-strain response of a $[\pm 45]_{2s}$ laminate under tensile loading. The model can predict the shear modulus degradation and permanent shear strain due to static loads, regardless of ply orientation. As long as damage is shear dominated, the match with experimental data is excellent. In follow-on work Ahmadi, Hajikazemi and van Paepegem

* Corresponding author.

E-mail address: c.kassapoglou@tudelft.nl (C. Kassapoglou).

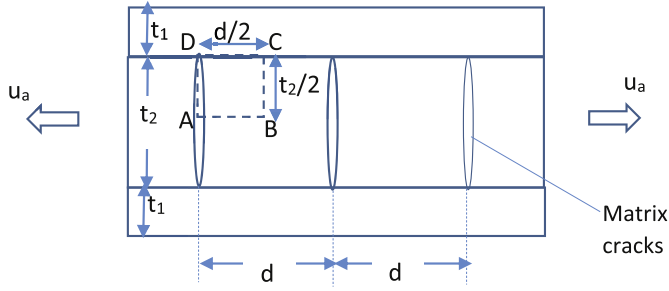


Fig. 1. Ply under transverse tension with matrix cracks at spacing d . Fibers in the cracked ply are perpendicular to the page.

[16], have used three dimensional finite element models and least square fits of numerical results from conservative RVEs to develop closed form expressions for laminate stiffnesses as a function of crack density. This approach requires a priori knowledge of crack density and relies on curve fitting to obtain the parameters in the stiffness equations.

Singh and Talreja [17], dealt with the problem of new crack creation in off-axis plies given an existing matrix crack pattern. They used test data of a reference laminate to obtain a parameter used in predicting new crack formation and a finite element model to determine crack-surface displacements. Varna further continued his contributions in this area by using a global-local approach combined with a stress-based approach for thick plies and a fracture mechanics approach for thin plies to model mechanical properties of laminates with matrix cracks [18]. Singh and Talreja [19], combined continuum damage mechanics with micromechanics while McCartney [20] used energy methods to model the stiffness of cracked plies.

Kashtalyan and Soutis [21] used a two dimensional shear lag model and equivalent constraints on the laminate to determine stiffness degradation for a given crack distribution accounting for longitudinal, transverse cracks and delaminations. The method requires knowledge of the location and size of cracks and solves iteratively a set of simultaneous non-linear equations. The required number of iterations increases with matrix crack density and delamination area.

In this paper a model is presented which attempts to combine accuracy with efficiency while accounting for the basic damage mechanisms which lead to stiffness degradation. Stresses in a cracked ply under in-plane loading are obtained exactly and in closed form including inelastic effects due to a non-linear shear stress-strain curve. An energy criterion is used to determine when the next crack appears. Ply and laminate-level elastic constants are obtained also in closed-form.

2. Approach

2.1. Ply under transverse tension

The cracks are assumed to be inside a laminate fully contained in the ply of interest. Such would be the case of a 90° ply surrounded by 0° plies but other ply orientations are possible. The laminate is under tension by an applied deflection u_a . It is also assumed that when the transverse in-situ strength is reached in the ply, a crack develops, that is, for matrix material under transverse tension, there is no inelastic

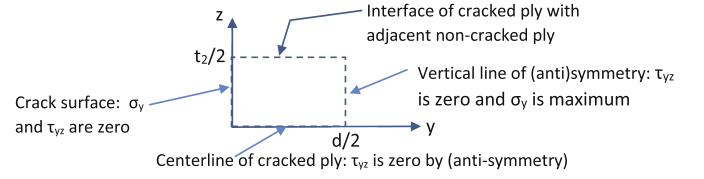


Fig. 2. Domain of the problem (fibers are perpendicular to the page).

behaviour prior to cracking. The situation is shown in Fig. 1 with three representative cracks spaced at a distance d .

It can be seen from Fig. 1 that the quadrant ABCD is a repeating unit within the cracked ply. Every portion of the cracked ply is either a mirror image or a parallel transposition of this quadrant with appropriate deflection and stress boundary conditions. Therefore, it suffices to solve the problem within this quadrant. The situation is shown in Fig. 2.

It is assumed that the structure in Fig. 2 is long in the x direction (perpendicular to the page) so there is no dependence of stresses on the x coordinate. As a result, the only stresses present are σ_y , τ_{yz} and σ_z . In the plane of Fig. 2, the cracked ply is isotropic. The stiffness is the same in all directions. As a result, using the equations of elasticity to eliminate strains and displacements leads to the well-known bi-harmonic equation:

$$\frac{\partial^4 \sigma_y}{\partial y^4} + 2 \frac{\partial^4 \sigma_y}{\partial y^2 \partial z^2} + \frac{\partial^4 \sigma_y}{\partial z^4} = 0 \quad (1)$$

with the boundary conditions:

$$\begin{aligned} \sigma_y &= 0 \text{ at } y = 0 \text{ (crack surface)} \\ \tau_{yz} &= 0 \text{ at } y = 0 \text{ (crack surface)} \\ \tau_{yz} &= 0 \text{ at } y = d/2 \text{ (symmetry)} \\ \tau_{yz} &= 0 \text{ at } z = 0 \text{ (antisymmetry)} \\ u &= u_o \text{ at } y = d/2 \end{aligned} \quad (2a-2e)$$

Note that the applied displacement u_o on face BC in Fig. 1 can be obtained as a function of the overall applied deflection u_a in Fig. 1, or the applied strain ϵ_a to the structure. The strain in each repeating unit is the same as the strain on the structure:

$$\frac{u_o}{(d/2)} = \epsilon_a = > u_o = \frac{\epsilon_a d}{2} \quad (3)$$

Equation (1) subject to boundary conditions (2a-2e) can be solved exactly. The solution is:

$$\sigma_y = \sum (A_{1n} e^{\varphi_n y} + A_{2n} y e^{\varphi_n y} + A_{3n} e^{-\varphi_n y} + A_{4n} y e^{-\varphi_n y}) \cos \frac{n\pi z}{t_2} + K \quad (4)$$

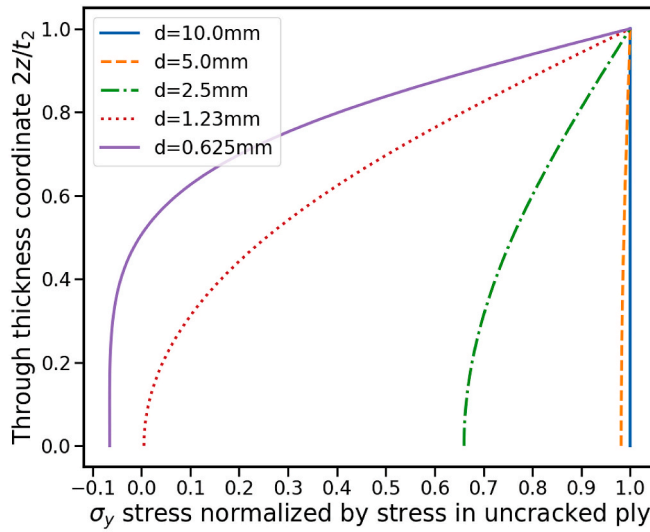
with n odd, and:

$$\varphi_n = \frac{n\pi}{t_2} \quad (5)$$

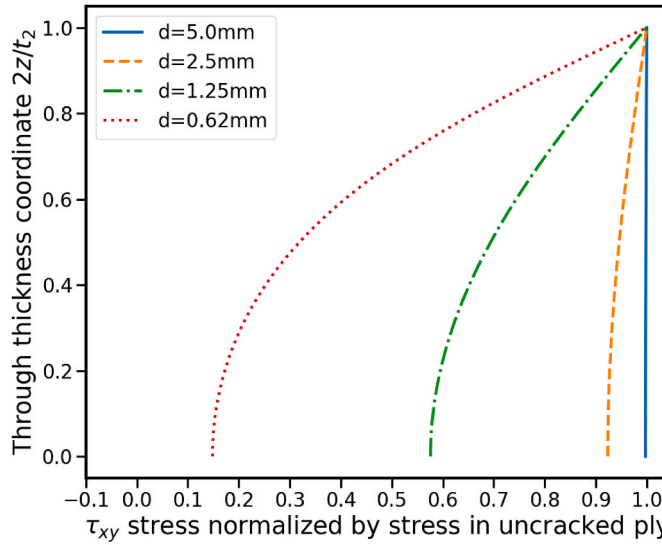
The constants K , A_{1n} , A_{2n} , A_{3n} and A_{4n} in eq (4) are obtained by first determining the remaining stresses through equilibrium and using the stress-strain and strain-displacement equations to determine the displacement u in the y direction so that eq. (3) can be applied. It can be shown that:

$$\tau_{yz} = \sum (A_{1n} \varphi_n e^{\varphi_n y} + A_{2n} (1 + \varphi_n y) e^{\varphi_n y} - A_{3n} \varphi_n e^{-\varphi_n y} + A_{4n} \varphi_n (1 - \varphi_n y) e^{-\varphi_n y}) \frac{t_2}{n\pi} \sin \frac{n\pi z}{t_2} \quad (6)$$

$$\sigma_z = - \sum ((A_{1n} \varphi_n^2 + 2A_{2n} \varphi_n) e^{\varphi_n y} + A_{2n} \varphi_n^2 y e^{\varphi_n y} + (A_{3n} \varphi_n^2 - 2A_{4n} \varphi_n) e^{-\varphi_n y} + A_{4n} \varphi_n^2 y e^{-\varphi_n y}) \left(\frac{t_2}{n\pi} \right)^2 \cos \frac{n\pi z}{t_2} \quad (7)$$



a. Through-thickness dependence of σ_y (applied strain = 0.006)



b. Through-thickness dependence of τ_{xy} (applied shear strain = 0.00476)

Fig. 3. Stresses at $y = d/2$ as a function of out-of-plane coordinate z in a cracked ply under (a) transverse tension or (b) shear.

Also, applying conditions (2a)-(2e) gives:

$$K = \frac{2u_0}{d} E_y = \epsilon_a E_y \tag{8}$$

where E_y is the ply Young's modulus perpendicular to the fibers, and:

$$A_{1n} = -\frac{(e^{-\varphi_n d} - 1 - \varphi_n d)}{(e^{-\varphi_n d} - e^{\varphi_n d} - 2\varphi_n d)} \frac{4K}{n\pi} \sin \frac{n\pi}{2} \tag{9}$$

$$A_{2n} = \frac{\varphi_n \left[e^{-\frac{\varphi_n d}{2}} - \frac{\varphi_n d}{2} \left(1 + \frac{\varphi_n d}{2} \right) - e^{-\frac{3\varphi_n d}{2}} \left(1 - \frac{\varphi_n d}{2} \right) \right]}{\left(\frac{\varphi_n d}{2} \left(1 + \frac{\varphi_n d}{2} \right) - \frac{-\varphi_n d}{2} \left(1 - \frac{\varphi_n d}{2} \right) \right) (e^{-\varphi_n d} - e^{\varphi_n d} - 2\varphi_n d)} \frac{4K}{n\pi} \sin \frac{n\pi}{2} \tag{10}$$

$$A_{3n} = \frac{(e^{\varphi_n d} - 1 + \varphi_n d)}{(e^{-\varphi_n d} - e^{\varphi_n d} - 2\varphi_n d)} \frac{4K}{n\pi} \sin \frac{n\pi}{2} \tag{11}$$

$$A_{4n} = \frac{\varphi_n \left[-e^{\frac{\varphi_n d}{2}} + \frac{-\varphi_n d}{2} \left(1 - \frac{\varphi_n d}{2} \right) + e^{\frac{3\varphi_n d}{2}} \left(1 + \frac{\varphi_n d}{2} \right) \right]}{\left(\frac{\varphi_n d}{2} \left(1 + \frac{\varphi_n d}{2} \right) - \frac{-\varphi_n d}{2} \left(1 - \frac{\varphi_n d}{2} \right) \right) (e^{-\varphi_n d} - e^{\varphi_n d} - 2\varphi_n d)} \frac{4K}{n\pi} \sin \frac{n\pi}{2} \tag{12}$$

It is interesting to note that the solution presented here does not require any assumption on the z dependence of the stresses as is typically done with some energy minimization solutions [6,22]. The actual z dependence of the stresses is a natural outcome of the solution process. For large d spacing, the in-plane stress σ_y is constant with z in each ply. For smaller d spacings this changes from nearly linear to very steep gradients as a function of z for very small d values. This change in z

dependence is shown in Fig. 3a for various d values.

The stress distribution in Fig. 3a is for the stress at $d/2$ (half-way between cracks) and was obtained for an applied transverse strain $\varepsilon_y = 0.006$. The plot in that Figure covers half of the thickness of the 90° ply (see Fig. 2) because of symmetry. The σ_y stress is lower everywhere else in the region between two successive cracks. The material properties used were $E_y = 12.76$ GPa and total thickness of 90° ply $t_2 = 1.12$ mm. It is interesting to note that for very short crack spacings, $d = 0.625$ mm for example, the σ_y stress becomes negative. This is necessary in order to generate the applied uniform deflection u_0 at $y = d/2$.

Another interesting observation which sheds some light to crack saturation is the change of the average stress at $y = d/2$ as d becomes smaller. The average σ_y stress at $d/2$ is obtained from eq. (4) as:

$$\sigma_{yav} = \frac{2}{t_2} \int_0^{t_2/2} \sigma_y \left(y = \frac{d}{2} \right) dz = \sum \left(A_{1n} e^{\varphi_n d/2} + A_{2n} \frac{d}{2} e^{\varphi_n d/2} + A_{3n} e^{-\varphi_n d/2} + A_{4n} \frac{d}{2} e^{-\varphi_n d/2} \right) \frac{2}{n\pi} \sin \frac{n\pi}{2} + K \quad (13)$$

For large values of d , the σ_y stress as a function of y rises from 0 to the value it would attain if there were no cracks present. Thus, for large d values, σ_y departs from the value a pristine ply would have only near the matrix cracks. This means there is a region between cracks of constant σ_y stress. As a result, the next crack would appear anywhere in that region of constant stress and originating at locations where defects (resin rich regions, voids) are present. This means that as new cracks are created the spacing will be random. If, however, the crack spacing is short enough, the region of maximum σ_y stress degenerates to a point, the mid-point between two successive cracks. Then the crack spacing becomes uniform and every time a crack appears it will be at $y = d/2$ half-way between cracks.

If the σ_y stress at $d/2$ is uniform with z , which is the case for large d , a crack will appear at that location when $\sigma_y (y = d/2) = Y_{is}^t$ with Y_{is}^t the in-situ transverse tension strength of the material. In-situ strength here refers to the stress at which a ply will first crack. This stress changes with location of the ply (inside the laminate or on the surface) and with ply thickness. If the σ_y stress at $d/2$ is not uniform with z (d is small) a simple maximum stress criterion is no longer accurate enough in predicting when the next full-depth crack will appear. A crack may start when $\sigma_y(d/2, z) > Y_{is}^t$ but if there is not enough energy available, it may not extend through the thickness of the 90° ply [23]. An energy criterion is used instead: If, at a specific location, the difference of the (average) energy density right after a crack is formed and the energy density right before crack formation reaches a critical value, a new crack will appear. The strain energy density is used instead of strain energy because the crack formation is a localized problem and the energy per unit volume is expected to be a better indicator of when the material reaches a critical state locally. This difference in energy density is evaluated at the point of maximum σ_y stress after crack formation as shown in Fig. 4. That point is at $d/4$ before the new crack appears at $d/2$. This same location after the crack appears is still at $d/4$, if the old crack spacing is used, but it will be the mid-point of the new crack spacing, which is now $d/2$. Using the average stress at that location, the condition for new crack formation is:

$$\left[U_{dav} \left(\frac{d}{4}, z \right) \right]_{before} - \left[U_{dav} \left(\frac{d}{4}, z \right) \right]_{after} = \Delta U_{davicrit} \quad (14)$$

where U_{dav} denotes the energy density per unit width (width measured along the x axis in Figs. 1 and 2) evaluated using average stress values

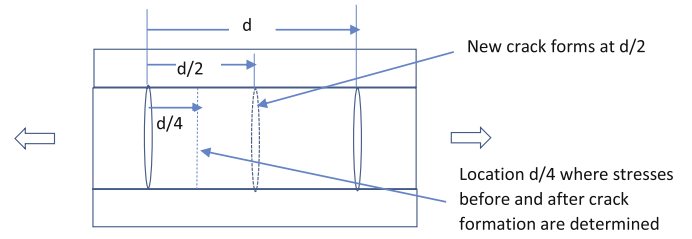


Fig. 4. Location for critical energy difference evaluation before and after crack creation at $d/2$.

and the subscripts “before” and “after” refer to crack formation. The

crack spacing d in eq. (14) refers to the original crack spacing before the new crack was created. The location $d/4$ is chosen because, after crack formation at $d/2$ it will have the highest stress σ_y and no shear stress τ_{yz} . Note that only half of the thickness t_2 of the 90° ply is used because of symmetry.

At the location of interest, $y = d/2$, the shear stress τ_{yz} is zero by symmetry or by substituting in eq. (6). Therefore, it does not directly contribute to crack formation at that location. Furthermore, σ_z , even if tensile in that region, will also not contribute to crack formation with cracks oriented as shown in Fig. 4. If anything, cracks caused by high tensile σ_z stress would be perpendicular to the ones shown in the Figure. As a result, the thickness-averaged energy density is given by:

$$U_{dav} = \frac{\sigma_{yav}^2}{2E_y} \quad (15)$$

Note that the transverse Young’s modulus E_y is always a constant between cracks and does not change. The presence of the cracks causes the ply to behave within the laminate with a different transverse modulus as will be shown below. Substituting in eq. (14) leads to:

$$\frac{1}{2E_y} \left[\left(\sigma_{yav}^2 \right)_{before} - \left(\sigma_{yav}^2 \right)_{after} \right] = \Delta U_{davicrit} \quad (16)$$

where, σ_{yav} before crack formation is evaluated at $d/4$ using eq. (18) and σ_{yav} after crack formation is evaluated using eq. (13) and d equal to half the value before crack formation. Recognizing that E_y is fixed for a given problem, eq. (16) becomes:

$$\left(\sigma_{yav}^2 \right)_{before} - \left(\sigma_{yav}^2 \right)_{after} = \Delta \sigma_{crit}^2 = 2E_y \Delta U_{davicrit} \quad (17)$$

The right hand side of eq. (17) can be determined by requiring that eq. (17) give the same prediction as a maximum stress criterion when cracks first appear in a pristine ply. This happens when the transverse stress in the ply equals the in-situ transverse strength of the material Y_{is}^t . Using equations (9)–(12) to substitute in eq. (13) it can be shown, after some manipulation, that:

$$\left(\sigma_{yav} \right)_{before} = \left(\sigma_{yav} \right)_{d/4} = K + \frac{8K}{\pi^2} \sum \frac{T_n}{B_n} \quad (18)$$

with n odd, K given by eq. (8) and,

$$T_n = \frac{1}{n^2} \left[\frac{e^{\frac{5\varphi_n d}{4}}}{2} \left(1 + \frac{3\varphi_n d}{4} + \frac{\varphi_n^2 d^2}{8} \right) - e^{-\frac{\varphi_n d}{4}} \left(1 + \frac{\varphi_n d}{4} - \frac{\varphi_n^2 d^2}{4} \right) + \frac{e^{\frac{3\varphi_n d}{4}}}{2} \left(1 + \frac{5\varphi_n d}{4} + \frac{3\varphi_n^2 d^2}{8} \right) - e^{\frac{\varphi_n d}{4}} \left(1 - \frac{\varphi_n d}{4} - \frac{\varphi_n^2 d^2}{4} \right) + \frac{e^{-\frac{5\varphi_n d}{4}}}{2} \left(1 - \frac{3\varphi_n d}{4} + \frac{\varphi_n^2 d^2}{8} \right) + \frac{e^{-\frac{3\varphi_n d}{4}}}{2} \left(1 - \frac{5\varphi_n d}{4} + \frac{3\varphi_n^2 d^2}{8} \right) \right] \quad (19)$$

$$B_n = \left[\frac{e^{\frac{\varphi_n d}{2}}}{2} \left(1 + \frac{\varphi_n d}{2} \right) - \frac{e^{-\frac{\varphi_n d}{2}}}{2} \left(1 - \frac{\varphi_n d}{2} \right) \right] (e^{-\varphi_n d} - e^{\varphi_n d} - 2\varphi_n d) \quad (20)$$

Similarly, it can be shown that:

$$(\sigma_{yav})_{after} = K + \frac{8K}{\pi^2} \sum \frac{1}{n^2} \frac{2e^{\frac{\varphi_n d}{4}} - 2e^{-\frac{\varphi_n d}{4}} + \frac{\varphi_n d}{2} \left(e^{\frac{\varphi_n d}{4}} + e^{-\frac{\varphi_n d}{4}} \right)}{\left(e^{-\frac{\varphi_n d}{2}} - e^{\frac{\varphi_n d}{2}} - \varphi_n d \right)} \quad (21)$$

Using equations (18)–(21) to substitute in eq. (17), the normalized quantity $\Delta\sigma^2/K^2$ can be determined for a range of values of the parameter $r = \pi d/t_2$ (note: $\varphi_n d = nr$). A plot of $\Delta\sigma^2/K^2$ as a function of r is shown as a continuous line in Fig. 5.

The curve in Fig. 5 has a maximum at $r_m = 9.3167$ with a value $(\Delta\sigma^2/K^2)_{max} = 0.27024$. This curve is independent of material and its basic shape will be the same for different values of the transverse strain applied to a ply. As the strain increases the curve would shift up and the maximum will still occur at the same r_m value. Therefore, when cracking first starts, the critical value of $\Delta\sigma^2/K^2$ corresponding to a transverse stress of Y_{is}^t acting in the ply will be given by the value of the maximum of the $\Delta\sigma^2/K^2$ curve when the applied strain causes a transverse stress equal to Y_{is}^t :

$$\Delta\sigma_{crit}^2 = 0.27024 (E_y \varepsilon_{crit})^2 = 0.27024 (Y_{is}^t)^2 \quad (22)$$

where eq. (8) was used to substitute for K and the fact that at the critical strain causing the first cracks, $Y_{is}^t = E_y \varepsilon_{crit}$.

If the applied strain is increased beyond ε_{crit} to a value ε_a , using the in-situ strength is no longer a reliable way to predict further matrix cracking. The critical energy density, however, can be used for any applied strain. And since the Young's modulus between cracks remains

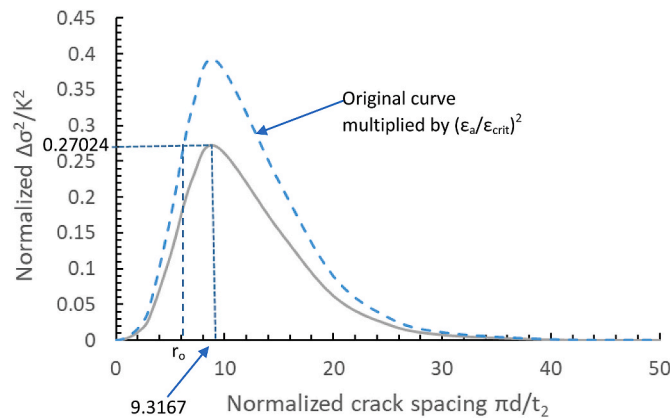


Fig. 5. Normalized average energy density $\Delta\sigma^2/K^2$ as a function of normalized crack spacing $\pi d/t_2$.

the same, the quantity $\Delta\sigma_{crit}^2$ determined in eq. (22) can be used. For a given applied strain ε_a , the continuous line in Fig. 5 is multiplied by the square of the ratio $\varepsilon_a/\varepsilon_{crit}$. This gives the dashed curve in Fig. 5 which intersects a horizontal line at $\Delta\sigma^2/K^2 = 0.27024$ at a point. The ordinate r_o corresponding to this intersection defines the new crack spacing $d_o = r_o t_2/\pi$ caused by applied strain ε_a . The determination of r_o and, through it, the new crack spacing d_o can be done in general for any material. By changing the ratio $\varepsilon_a/\varepsilon_{crit}$ successive points r_o as described in Fig. 5 can be found. Thus, the dependence of r_o to the applied strain can be found as a single master curve independent of material, surrounding layup and thickness of the cracked ply. This d/t_2 dependence is shown in Fig. 6.

The cracked ply inside a laminate will behave as if its Young's modulus perpendicular to the fibers E_{yr} is obtained by dividing the average stress at $d_o/2$ by ε_a :

$$E_{yr} = \frac{(\sigma_{yav})_{d_o/2}}{\varepsilon_{ya}} = \frac{1}{\varepsilon_{ya}} \left(K + \frac{8K}{\pi^2} \sum \frac{1}{n^2} \frac{2e^{\frac{\varphi_n d_o}{4}} - 2e^{-\frac{\varphi_n d_o}{4}} + \varphi_n d_o \left(e^{\frac{\varphi_n d_o}{4}} + e^{-\frac{\varphi_n d_o}{4}} \right)}{\left(e^{-\varphi_n d_o} - e^{\varphi_n d_o} - 2\varphi_n d_o \right)} \right) \quad (23)$$

Substituting for K from equation (8) it can be shown that the reduced Young's modulus due to the presence of cracks, normalized by the pristine Young's modulus is given by:

$$\frac{E_{yr}}{E_y} = \left(1 + \frac{8}{\pi^2} \sum \frac{1}{n^2} \frac{2e^{\frac{\varphi_n d_o}{2}} - 2e^{-\frac{\varphi_n d_o}{2}} + \varphi_n d_o \left(e^{\frac{\varphi_n d_o}{2}} + e^{-\frac{\varphi_n d_o}{2}} \right)}{\left(e^{-\varphi_n d_o} - e^{\varphi_n d_o} - 2\varphi_n d_o \right)} \right) \quad (24)$$

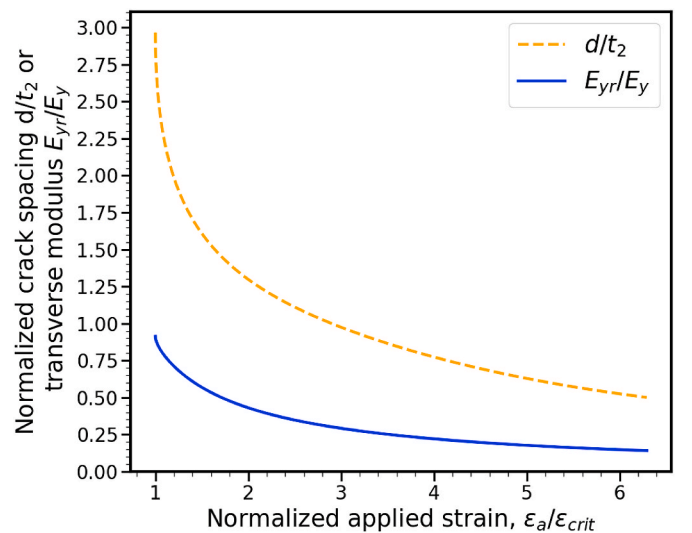
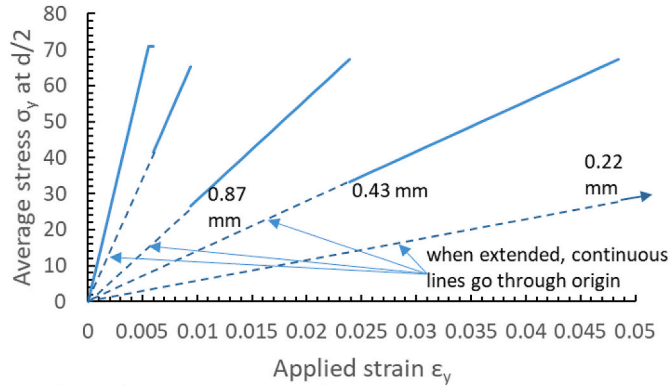


Fig. 6. Crack spacing and transverse Young's modulus as a function of strain for any material.

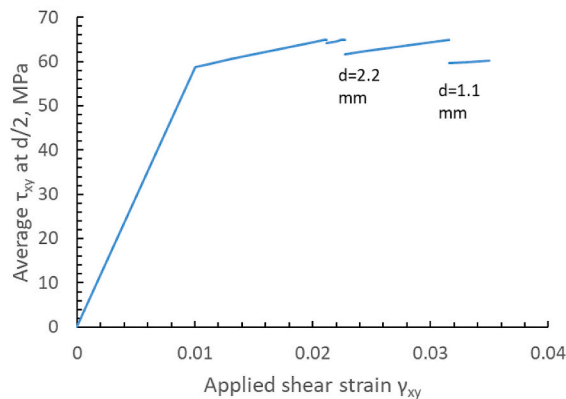
Table 1
Material properties used for comparisons to test results.

Property	Fig. 8a–c, 13–15		Figs. 11a and 12		Fig. 11c		Fig. 11b	
	Value	Source	Value	Source	Value	Source	Value	Source
E_x (GPa)	44.73	[24]	38.9	[14]	138.0	[31]	138.0	[30]
E_y (GPa)	12.76	[24]	13.3	[14]	10.3	[31]	11.0	[30]
G_{xy} (GPa)	5.83	[24]	5.13	[14]	6.5	[29]	5.52	[29]
ν_{xy}	0.297	[24]	0.258	[14]	0.3	[31]	0.28	[30]
τ_y (MPa) ^a	56.09	[30]	45.18	[15]	56.78	[29]	62.56	[29]
Y_{is}^t (MPa) ^a	70.96	[10]	36.5	[14]	25.58	[29]	38.78	[29]
k (GPa) ^a	0.556	[30]	0.127	[15]	0.332	[29]	0.343	[29]
S_{is} (GPa) ^a	73.0	[30]	70.1	[15]	146.53	[29]	90.25	[29]

^a Value derived from data within given reference.



a. Ply under transverse strain



b. Ply under shear strain

Fig. 7. Maximum stress at mid-point between cracks as a function of applied strain.

Knowing d_0 through r_0 in Fig. 5, allows determination of the ratio of the transverse Young's modulus of the cracked ply to the pristine modulus through equation (24). A master curve, independent of material and stacking sequence of surrounding plies can thus be obtained and is also shown in Fig. 6.

The two curves in Fig. 6 give the crack spacing and transverse Young's modulus of a cracked ply for any material. It should be noted that for comparisons with crack spacing measured from test, twice the value from Fig. 6 should be used because, for a given strain, d corresponds to the moment new cracks will be created and it is unlikely test measurements capture exactly that moment. More likely, each crack density measurement captures the crack state prior to the next crack creation. One of the advantages of the present approach is that these quantities are obtained essentially in closed form for any material. Thus, the method can be easily used in numerical simulations to track and update local stiffness by determining local strains and applying equations (18)–(21) and (24) to almost instantaneously update stiffness at a

given load level.

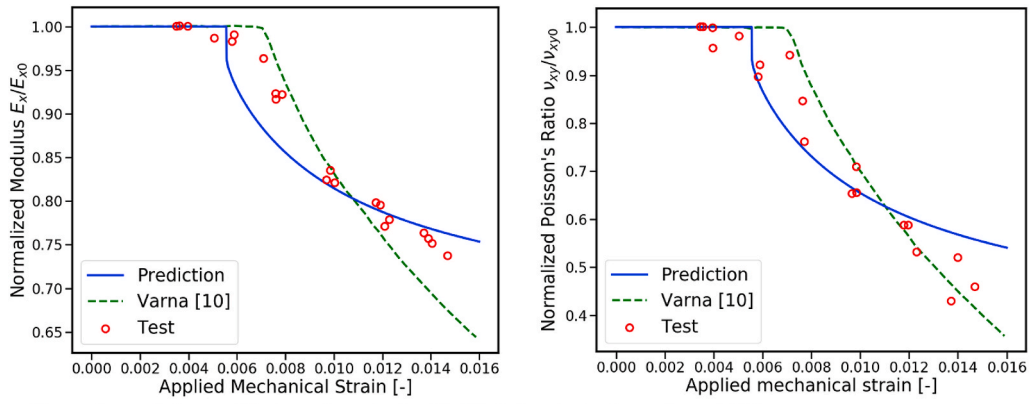
One interesting conclusion from Figs. 5 and 6 is what happens right after the first cracks are created. According to Fig. 5, cracks will be randomly distributed until $r = 9.3167$. This corresponds to a crack spacing $d = 2.966t_2$. Beyond that point, new cracks will appear at the mid-point of the previous crack spacing. This is in agreement with the observation made earlier that the first few cracks will be widely spaced allowing the σ_y stress to rise to the value it would have if there were no cracks, i.e. Y_{is}^t , thus causing more cracks until the spacing is short enough such that the maximum σ_y stress between cracks is now less than Y_{is}^t and crack creation stops.

Further implications can be seen through an example. Consider a typical glass/epoxy material such as the one used in Ref. [9,10] with properties given in Table 1. In this case, eq. (22) gives $\Delta\sigma_{crit}^2 = 1360.7 \times 10^{12} \text{ MPa}^2$ and $\epsilon_{crit} = 0.00556$ microstrain. The response of a ply under transverse strain $\epsilon_a > \epsilon_{crit}$ (or multiple consecutive plies of the same orientation) can be obtained by applying equations (18)–(21) to find the r_0 value shown in Fig. 5 for each value of ϵ_a . The results are shown in Fig. 7a for a total thickness of 90° plies of 1.12 mm (8-ply stack).

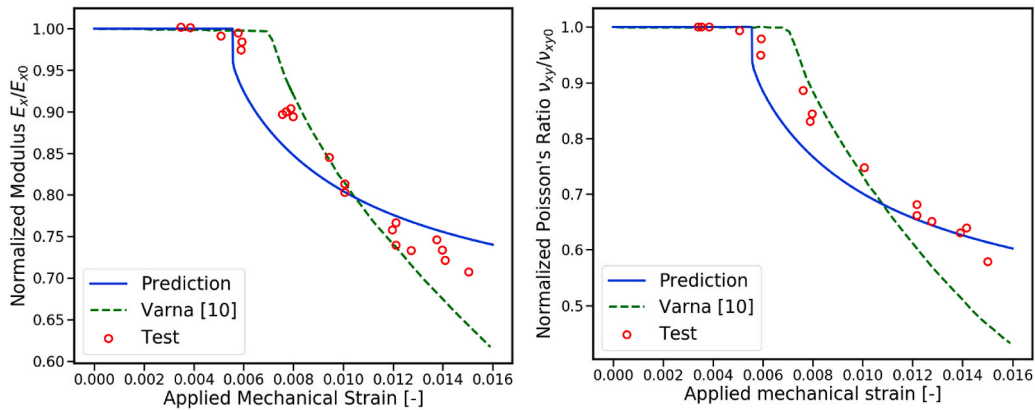
The graph of Fig. 7a consists of linear segments interrupted every time a new crack forms. The values of d after each crack formation are included in Fig. 7a next to the bottom end of each inclined continuous line. After a crack forms, the strain is increased and a new continuous line is traced until the next crack is created at the mid-point of the previous crack spacing. It can be shown that all the inclined portions of the graph, when extended as indicated by the dashed lines, go through the origin. This means that if the ply were completely unloaded (applied strain $\epsilon_y = 0$), the strain anywhere between cracks would go to zero. This, as will be shown later, is different than what happens for shear loading where the ply may have inelastic behaviour prior to cracking.

Therefore, the average stress σ_y at any point between cracks is linearly related to the applied strain with a slope equal to the slope of the inclined portion of the curve in Fig. 7a connecting the origin with the point where a crack occurs for a given strain. This is in agreement with eq. (23) which assumed linear stress-strain behaviour as stress is raised from 0 to the stress which would cause a new crack to form. Note that the maximum stress at which new cracks form, the upper end of each inclined segment, is not equal to Y_{is}^t but a lower value. Only for strains very close to 0.00556, when the first cracks appear, will the maximum stress equal Y_{is}^t . If the crack spacing is small, there is not enough distance between cracks for the shear lag problem to fully develop. The cracked ply partially “unloads” to the adjacent uncracked plies and the maximum stress at $d/2$, when averaged over the ply thickness, is lower than what it would be for large crack spacing. This does not mean that the point stress as a function of the out-of-plane coordinate z is lower than Y_{is}^t . As shown in Fig. 3a, the stress as a function of z is very non-linear for short crack spacings. In fact, it can exceed Y_{is}^t near the interface with the uncracked plies. The maximum stress averaged with respect to z , however, will not exceed Y_{is}^t and for short crack spacings will even be lower. The maximum (average) stress values in Fig. 7a are, for the different segments: 70.96, 70.96, 65.15, 67.37 and 67.36 MPa.

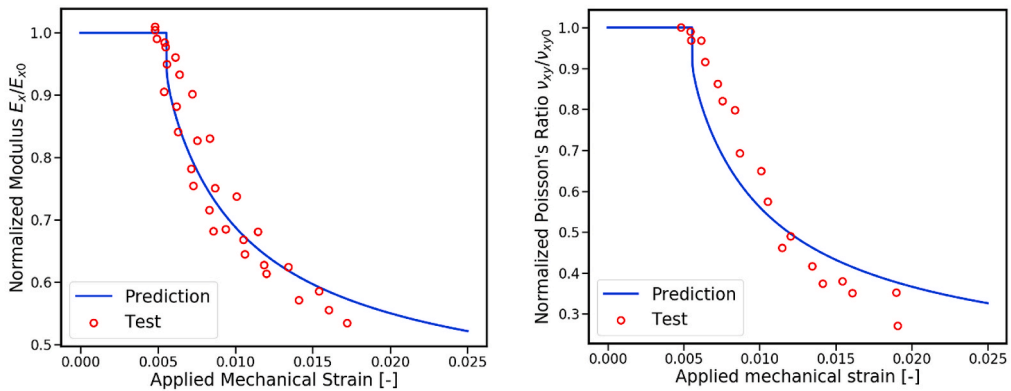
There is a short horizontal portion at the end of the first inclined



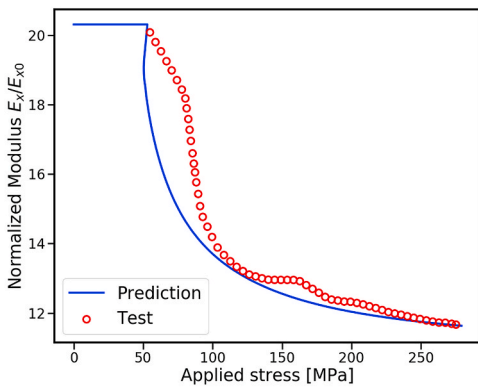
a. Young's modulus and Poisson's ratio for $[0_2/90_4]_s$ laminate (tests from [10])



b. Young's modulus and Poisson's ratio for $[\pm 15/90_4]_s$ laminate (test results from [10])



c. Young's modulus and Poisson's ratio for $[0/90_8/0]_s$ laminate (test results from [9])



d. Young's modulus for $[0/90_3]_s$ laminate (test results from [4])

Fig. 8. Comparison of present model to experimental results.

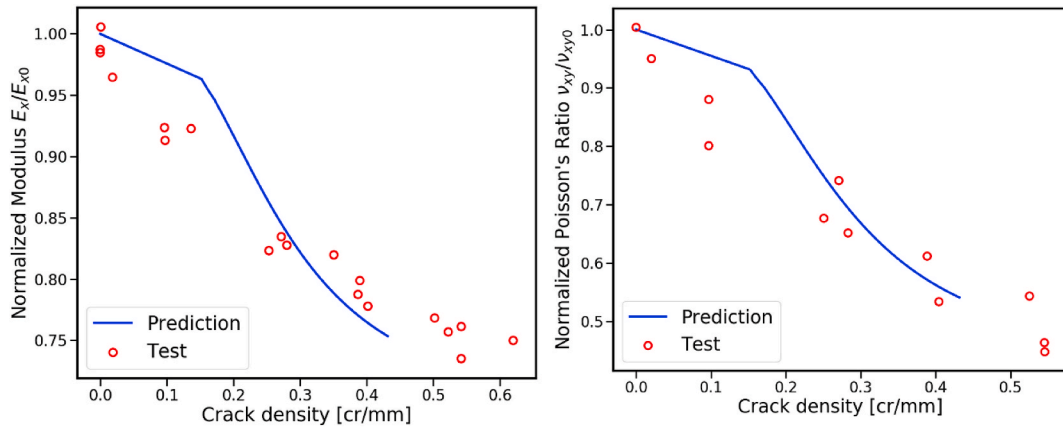


Fig. 9. Young's modulus and Poisson's ratio for $[0_2/90_4]_s$ laminate as a function of crack density (test results from Ref. [10]).

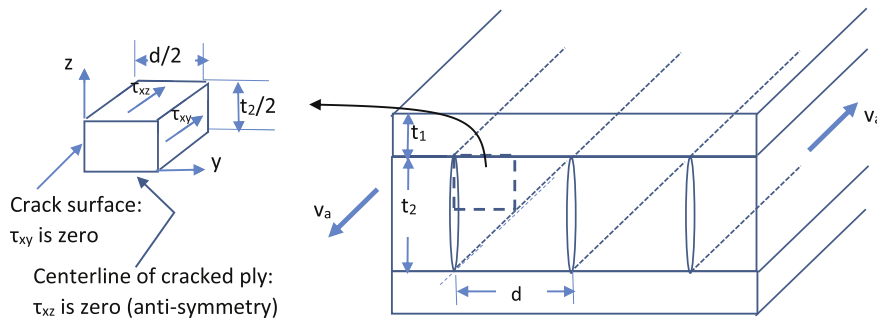


Fig. 10. Matrix cracks forming in a ply under pure shear.

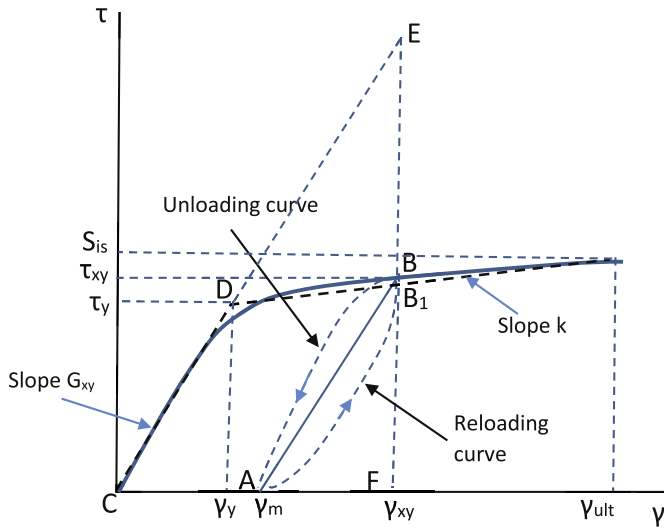


Fig. 11. Shear stress-strain curve approximated by bi-linear curve.

segment in Fig. 7a. This is because the crack spacing is large enough in this region for the maximum stress between cracks to reach γ_{is}^I . It should be emphasized that each inclined segment in Fig. 7a corresponds to a different point in the ply, the location where a new crack will appear. For this reason, the inclined lines are not connected with vertical segments.

Once the material properties in Table 1 are fixed, the reduced Young's modulus in the transverse direction will not change with layup. The layup factors in only indirectly if the laminate is under generalized loading where it will be used in order to obtain the transverse strain ϵ_{ya}

in the ply of interest. In a sense, for a given material and ply thickness, which largely fix γ_{is}^I , and through it $\Delta U_{dacr,cr}$, one can use the curve of Fig. 6 to generate a line of reduced Young's modulus E_{yr} as a function of ϵ_{ya} and, for a given strain value, read off the value of E_{yr} . This means that once matrix cracks appear the reduced stiffness is not a constant value as is often assumed in numerical progressive failure analyses, but is a function of the local transverse strain ϵ_{ya} .

An interesting observation can be made here about crack saturation. If crack saturation is defined as the crack density beyond which a cracked ply cannot transfer any load, then the present approach suggests that this point will be reached only when the crack opening displacement at the middle of the ply, at $y = 0$ and $z = 0$ in Fig. 2, equals half the crack spacing $d/2$. This can be calculated in closed form with the present model and, for the case of Fig. 7a, this would occur for an approximate crack spacing $d = 0.04$ mm. The smallest d value in Fig. 7a is 0.22 mm corresponding to an approximate applied strain of 0.048. Clearly, the ply or the laminate will have failed before this point is reached. As is seen in Fig. 7a, as the applied strain increases, it takes a much higher strain to cause the next crack to form. For example, if an applied strain of 0.022 is reached, corresponding to a crack spacing of 0.43 mm, no more cracks would appear until the strain increased to 0.048 (to get a value of $d = 0.22$ mm). Usually, in tests like this, either the test is stopped before such high strains are reached or other failure modes appear (e.g. delaminations and fiber breakage) leading to final specimen failure before such high strains are reached. As a result, the relatively large strain range over which no more cracks appear tends to be interpreted as crack saturation. Based on this argument, it would appear in Fig. 7a that crack saturation has been reached in the range $d = 0.87$ – 1.73 mm which is in line with the high end of crack densities reported by Ryder and Crossman [25] for Graphite/Epoxy and Varna and Berglund [26] for Glass/Epoxy and Graphite/Epoxy.

The value of E_{yr} obtained by eq. (24) can be used in classical laminated plate theory to obtain the reduced laminate stiffness for a given

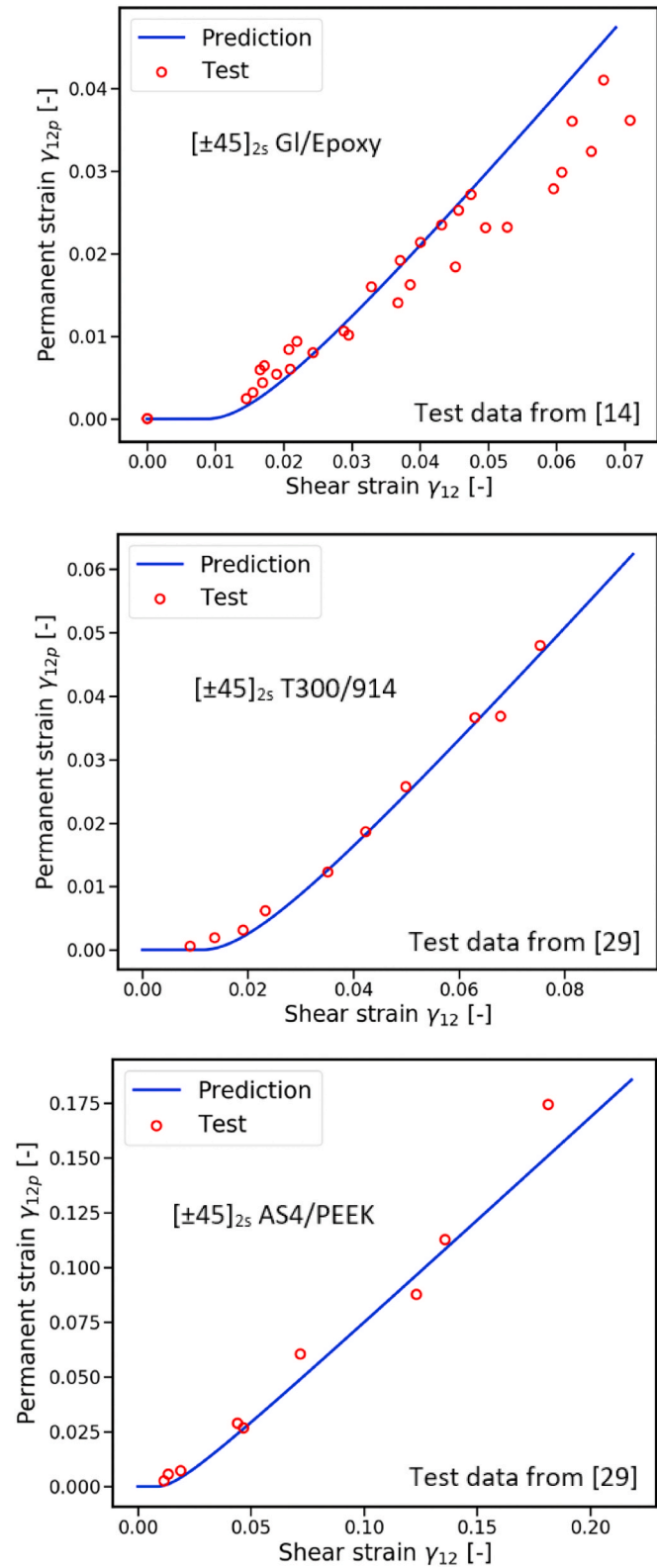


Fig. 12. Comparison of predicted permanent shear strain to test results in Ref. [14,29].

material. Furthermore, by solving for the minor Poisson's ratio of the cracked ply:

$$\nu_{yx} = \frac{E_{yr}}{E_x} \nu_{xy} \quad (25)$$

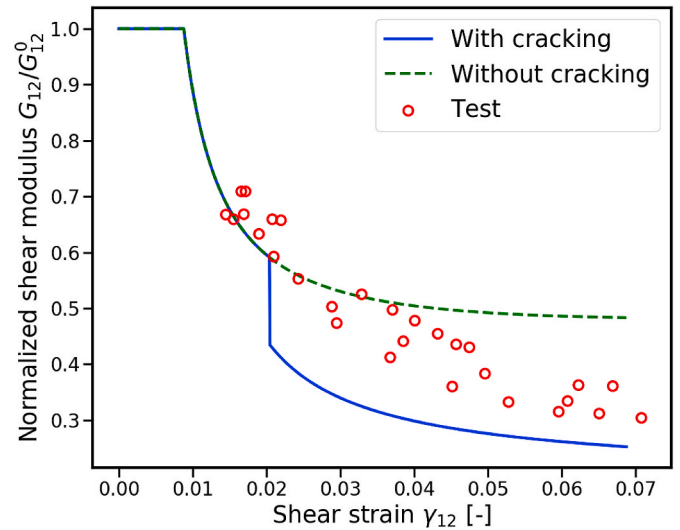


Fig. 13. Normalized shear modulus predictions compared to tests in Ref. [14].

and using classical laminated plate theory, the laminate major Poisson's ratio can be obtained.

For the materials in Table 1, the predictions of the present method are compared to test results from Ref. [4,9,10] in Fig. 8.

It is seen from Fig. 8 that the predictions of the present method are in very good to excellent agreement with test results. In addition, the predictions by Varna et al. [10] are also shown in Fig. 8a and b showing somewhat higher accuracy in Fig. 8a but the present method is more accurate in Fig. 8b, in particular at higher applied strains. Small discrepancies between the present method and test results could be due to several issues: The value of Y_{is}^I used may not be sufficiently accurate. A modified criterion accounting for the delaying effect of compressive stresses could be more accurate. It should also be noted that comparisons of Young's modulus and Poisson's ratio versus crack density plots showed similar degree of accuracy except for a couple of cases where it was not clear at what strain level some cracks appeared during test. An example is shown in Fig. 9.

2.2. Ply under shear

As for the case under transverse tension, the matrix cracks created under shear are assumed to be confined in the ply in question. However, unlike the transverse shear case where the stress-strain curve is linear to failure, the shear stress-strain curve is assumed to be non-linear. The situation is shown in Fig. 10.

As before, there is no dependence on the x coordinate and the isolated quadrant repeats throughout the cracked ply and this allows the problem to be solved only within each quadrant. In general, the shear stress-strain relations are:

$$\begin{aligned} \tau_{xy} &= G_{xy} \gamma_{xy} \\ \tau_{xz} &= G_{xz} \gamma_{xz} \end{aligned} \quad (26a-b)$$

For most composite materials, the two shear moduli G_{xy} and G_{xz} are equal. Combining the two stress-strain equations with one equilibrium equation:

$$\frac{\partial \tau_{xy}}{\partial y} + \frac{\partial \tau_{yz}}{\partial z} = 0 \quad (27)$$

and the compatibility equation:

$$\frac{\partial \gamma_{xy}}{\partial z} = \frac{\partial \gamma_{yz}}{\partial y} \quad (28)$$

leads to the following governing equation for τ_{xy} :

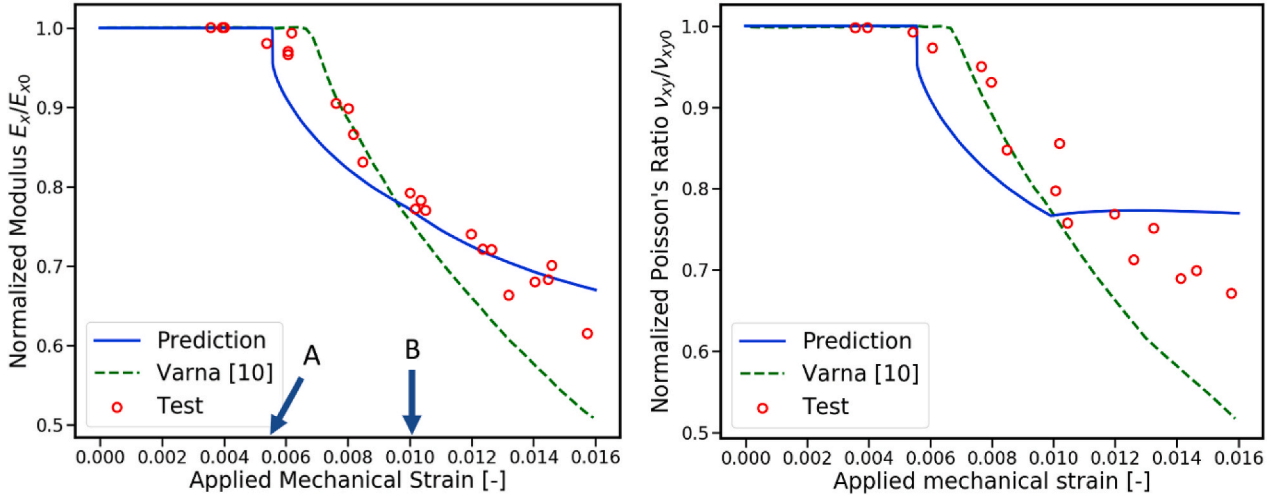


Fig. 14. Laminate modulus and Poisson's ratio predictions compared to test results for a $[\pm 30/90]_s$ laminate from Ref. [10].

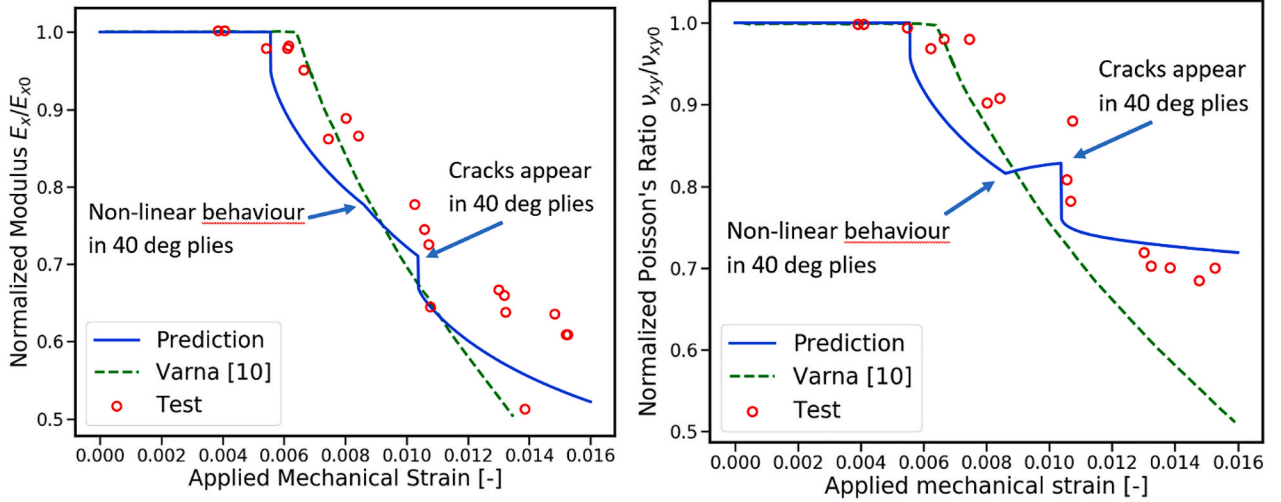


Fig. 15. Laminate stiffness predictions compared to test results from Ref. [10] for $[\pm 40/90]_s$.

$$\frac{\partial^2 \tau_{xy}}{\partial y^2} + \frac{\partial^2 \tau_{xy}}{\partial z^2} = 0 \quad (29)$$

This equation is to be solved subject to the boundary conditions:

$$\begin{aligned} \tau_{xy}(y=0) &= 0 \\ \tau_{xz}(z=0) &= 0 \\ v &= v_o \text{ at } y = d/2 \end{aligned} \quad (30a-c)$$

The prescribed deflection v_o at $d/2$ can be determined as a function of the applied shear strain γ_a :

$$v_o = \frac{\gamma_a d}{2} \quad (31)$$

The solution can be shown to be:

$$\tau_{xy} = -\frac{8v_o G_{xy}}{d} \sum \frac{\sin \frac{n\pi}{2}}{(1 + e^{k_n d}) n\pi} (e^{k_n y} + e^{k_n d} e^{-k_n y}) \cos \frac{n\pi z}{t_2} + \frac{2v_o}{d} G_{xy} \quad (32)$$

$$\tau_{xz} = \frac{8v_o G_{xy}}{d} \sum \frac{t_2}{(n\pi)^2 k_n} \frac{\sin \frac{n\pi}{2}}{(1 + e^{k_n d})} (e^{k_n y} - e^{k_n d} e^{-k_n y}) \sin \frac{n\pi z}{t_2} \quad (33)$$

where n is odd and:

$$k_n = \frac{n\pi}{t_2} \quad (34)$$

The distribution of τ_{xy} as a function of z for different values of the crack spacing d is shown in Fig. 3b. As for the case of the transverse stress, for large values of d the shear stress is constant through the thickness. For smaller d values the distribution is very non-linear. One important difference, compared to the case of transverse stress, is that the shear stress-strain curve may be non-linear. This means that, for sufficiently high loads, permanent shear strains are present in the ply [27–29]. The permanent strain must be known so that the new shear modulus, the slope of the line AB in Fig. 11, can be determined. Point A defines the permanent strain γ_m left in the structure if it were unloaded from point B down to zero stress. In what follows, it will be assumed that the shear stress-strain curve can be approximated by a bi-linear curve with initial slope G_{xy} and final slope k (see Fig. 11). The final slope k is obtained by ensuring that the areas under the bi-linear curve and the experimentally obtained stress-strain curve are the same.

Two quantities are now defined. The first is the “unavailable” elastic energy which is not available because of the non-linearity of the stress-strain curve. For an applied strain γ_{xy} , this is the area of the triangle DEB_1 in Fig. 11. Note that B_1 is on the bilinear approximation to the actual shear stress strain curve while B is on the actual stress-strain curve, both corresponding to the applied shear strain γ_{xy} . The second quantity is the “non-recoverable” strain energy because unloading from point B does not go to zero strain but to the permanent strain γ_m . This is

the area of the polygon CAB₁D.

The permanent shear strain γ_m is obtained by requiring that the ratio of the “unavailable” elastic energy to the total elastic energy (area CEF) is the same as the ratio of the “non-recoverable” energy to the total elastic-plastic energy (area CFB₁D). Substituting and solving for γ_m leads to:

$$\frac{DEB_1}{CEF} = \frac{CAB_1D}{CFB_1D} \Rightarrow \gamma_m = \frac{(G_{xy}\gamma_{xy} - \tau_{xy})(\gamma_{xy} - \gamma_y) [\tau_{xy}(\gamma_{xy} - \gamma_y) + G_{xy}\gamma_{xy}\gamma_y]}{G_{xy}\gamma_{xy}^2(\tau_{xy} + G_{xy}\gamma_y)} \quad (35)$$

In eq. (35), γ_{xy} is the applied strain and γ_y is the yield strain in shear for the ply material (see Fig. 11). The stress τ_{xy} corresponds to γ_{xy} and is obtained from the bi-linear stress-strain curve:

$$\tau_{xy} = G_{xy}\gamma_y + k(\gamma_{xy} - \gamma_y) \quad (36)$$

Then, the shear modulus due to the non-linearity of the stress-strain curve is the slope of line AB₁:

$$G_{xyr} = \frac{\tau_{xy}}{(\gamma_{xy} - \gamma_m)} \quad (37)$$

An indication of the accuracy of eq. (37) can be obtained by comparing the predictions of this method to test results by van Paepegem et al. [14] and Lafarie-Frenot and Touchard [29]. These comparisons are shown in Fig. 12. The agreement with tests from Ref. [14] is very good and with tests from Ref. [29] it is excellent.

In addition to the inelastic behaviour just discussed, matrix cracks will appear if the shear stress is sufficiently high. In a manner analogous to the case of transverse tension in the previous section, a crack would appear when:

$$\frac{[\tau_{xyavbefore}^2 - \tau_{xyavafter}^2]}{2G_{xy}} = \frac{\Delta\tau^2}{2G_{xy}} = \Delta U_{daverit} \quad (38)$$

where the average shear stress is evaluated at its maximum location after a crack appears, at $y = d/4$. The subscripts “before” and “after” refer to the stresses before and after a crack is created at the location of interest. Note that, unlike the case of transverse tension where E_y is constant, G_{xy} in eq. (38) is not and will be given by eq. (37) to reflect non-linearities in the shear stress-strain response. In a manner analogous to the case of transverse strain, the value of $\Delta U_{daverit}$ is obtained by finding the maximum of the $\Delta\tau^2$ curve as a function of d/t_2 when the applied shear strain causes a shear stress equal to the in situ shear strength S_{is} of the material. From equation (30) the average shear stress value over z used in equation (38) is obtained as:

$$\tau_{xyav} = -\frac{16\nu_o}{d}G_{xy} \sum \frac{(e^{k_n y} + e^{k_n d} e^{-k_n y})}{(1 + e^{k_n d})(n\pi)^2} + \frac{2\nu_o}{d}G_{xy} \quad (39)$$

if the shear stress is elastic for all z at the y location of interest, and

$$\tau_{xyav} = -\frac{16\nu_o}{d} \sum \frac{(e^{k_n y} + e^{k_n d} e^{-k_n y})}{(1 + e^{k_n d})(n\pi)^2} \left(k + (G_{xy} - k) \sin \frac{n\pi}{2} \sin \frac{n\pi z_o}{t_2} \right) + \frac{2\nu_o}{d} G_{xy} \left(\frac{2z_o}{t_2} + \frac{k}{G_{xy}} \left(1 - \frac{2z_o}{t_2} \right) \right) + G_{xy} \gamma_y \left(1 - \frac{k}{G_{xy}} \right) \left(1 - \frac{2z_o}{t_2} \right) \quad (40)$$

if the shear stress becomes non-linear for the portion $z_o \leq z \leq t_2/2$. The value of z_o is found as the value of z for which the right hand side of equation (32) equals the “yield” shear stress $G_{xy}\gamma_y$. Equations (39) or (40) are evaluated at the value of y in question.

The average shear stress for a ply with matrix cracks is shown in Fig. 7b. As for the transverse strain, the vertical discontinuities

correspond to crack creation. Because of the non-linear behaviour of the shear stress-strain curve, the magnitude of strain required to cause a new crack is greater than in the case of transverse strain. As a result, typically, the crack spacing corresponding to a shear strain is greater than for transverse strain of the same magnitude. The shear modulus G_{xy} in a cracked ply is given by equation (37) but now using the average shear stress at $d/2$ right before cracking:

$$G_{xyr} = \frac{\tau_{xyav}}{(\gamma_{xy} - \gamma_m)} \quad (41)$$

The presence of cracks, in general, reduces the shear stress to below the value it would attain if cracks were not present. This can be seen by substituting in equation (32). This means that the value of permanent strain γ_m in eq. (41) must correspond to the τ_{xyav} of interest and it would be different than the value used in eq. (37). As a result, a new shear stress-strain curve must be generated every time cracks appear in a ply. This is obtained by drawing a line parallel to the initial linear portion of the curve and a line of slope k going through the current value of τ_{xyav} at $d/2$. Note that if cracks are created in a ply due to shear strains, the transverse modulus E_{yr} must also be obtained following the procedure outlined in the previous section.

An important question is how the shear stress non-linearity interacts with matrix cracks. Typically, the non-linearities happen first, at least when a ply is under pure shear. If the shear strain in the ply increases sufficiently, matrix cracks will appear and they will affect or modify the non-linear behaviour. Several possibilities exist for modeling this interaction. At one extreme, neglecting the creation of matrix cracks will over-predict the actual shear modulus in the ply. At the other extreme, combining the two in sequence without interaction will compound their effect and is expected to under-predict the shear modulus. This can be seen in Fig. 13 where predictions from the two approaches are compared to test results from van Paepegem et al. [14]. As suggested, the two extreme approaches for predicting the shear modulus bracket the test data. In subsequent sections, wherever shear strains are present, first the complete inelastic behaviour is assumed by calculating the permanent shear strain corresponding to the applied laminate strains and then the effects of matrix cracking, if present, are accounted for. This is arbitrary and a better approach for the interaction of the two phenomena is needed where, for example, the applied strains are increased incrementally and both effects are included to determine the new moduli for each ply and continue increasing the applied strains. However, as will be shown, this approach captures the response quite accurately.

2.3. Ply under combined shear and transverse tension

Equations (16) and (38) are now combined to predict when a crack will be created at the location of maximum transverse and shear stresses which is at $d/2$:

$$\frac{[\sigma_{yavbefore}^2 - \sigma_{yavafter}^2]}{2E_y} + \frac{[\tau_{xyavbefore}^2 - \tau_{xyavafter}^2]}{2G_{xy}} = \Delta U_{daverit} \quad (42)$$

The value of $\Delta U_{daverit}$ will be different for different combinations of transverse and shear strains applied to the ply in question. If the ply-level load combination and thickness t_2 are fixed, $\Delta U_{daverit}$ will not

change with load intensity. The value of $\Delta U_{d\text{avcrit}}$ for a given load ratio of $\varepsilon_y/\gamma_{xy}$ and t_2 is obtained as the value of $\Delta U_{d\text{av}}$ corresponding to the case where, for large d when the stresses through the thickness are (nearly) uniform, a Hashin-type failure criterion [23] would predict local failure:

$$\frac{\sigma_{y\text{av}}^2}{(Y'_{is})^2} + \frac{\tau_{xy\text{av}}^2}{(S_{is})^2} = 1 \quad (43)$$

At this point, the use of this criterion is a matter of convenience. Other criteria, stress, or energy-based, which may be more representative of the mechanism of crack initiation, can be used. The stiffness of a laminate with plies under combined transverse (perpendicular to the fibers) and shear strains is obtained by using Classical Laminated-Plate Theory but modifying E_y , ν_{yx} and G_{xy} of each ply as necessary, according to eqs (24), (25) and (37).

The approach can be demonstrated better through an example. A $[\pm 30/90_4]_s$ fiberglass laminate under tension is used as the example. The material properties are the same as in Table 1. The applied axial strain ε_a is the same as the transverse strain in the 90° plies. As the applied strain increases, nothing happens until it reaches the value 0.00556 calculated in section 2.1. At that point the first cracks appear in the 90° plies. From then on, the laminate as a whole behaves as if the E_y value for the 90° plies is given by eq. (24).

The transverse and shear strains in the ply axes in the 30° and -30° plies are given by transforming the strains in the laminate axes which, in turn, are obtained from Classical Laminated Plate Theory:

$$\varepsilon_y(\theta) = \left[\sin^2\theta + \frac{\alpha_{12}}{\alpha_{11}}\cos^2\theta - 2\frac{\alpha_{16}}{\alpha_{11}}\sin\theta\cos\theta \right] \varepsilon_a \quad (44)$$

$$\gamma_{xy}(\theta) = \left[-2\sin\theta\cos\theta + 2\sin\theta\cos\theta\frac{\alpha_{12}}{\alpha_{11}} + (\cos^2\theta - \sin^2\theta)\frac{\alpha_{16}}{\alpha_{11}} \right] \varepsilon_a \quad (45)$$

where α_{11} , α_{12} , and α_{16} are the corresponding entries of the inverse of the

ABD matrix (with $\alpha_{16} = 0$ for a balanced laminate as in the present example) and θ the angle of the ply in question (30° or -30° in the present example).

As ε_a increases, a point is reached where $\gamma_{xy}(30)$ and $\gamma_{xy}(-30)$ reach, in absolute value, $\tau_y/G_{xy} = 0.01015$. At that point, the shear stress-strain response of the ± 30 plies becomes non-linear and eq. (37) is used to update G_{xy} . Whenever E_y in the 90 plies or G_{xy} in the ± 30 plies are updated, α_{11} , α_{12} , and α_{16} in eqs (44) and (45) must also be updated to get the "current" ε_y and γ_{xy} values in the ± 30 plies. This means that an iteration is necessary. As long as no cracks appear in the ± 30 plies, the laminate Young's modulus can be obtained via Classical Laminated-Plate Theory using the current values of E_y in the 90 plies and G_{xy} in the ± 30 plies. It should be noted that the presence of cracks in the 90 plies means the value of G_{xy} in these plies has also changed. This can be calculated following the approach described below but it is not needed for calculating the axial modulus of this particular laminate. As ε_a is increased further, a point is reached when eq. (43) is satisfied. This means matrix cracks appear in the ± 30 plies. To use eq. (43), the in-situ strength S_{is} of the material is needed. For the present material, this is calculated as the shear stress that the bi-linear curve described by G_{xy} and k gives for the failure strain of 0.04. The result is $S_{is} = 73$ MPa.

The predictions of the present method are compared to test results by Varna et al. [10] in Fig. 14. Material properties are the same as in Table 1 with S_{is} as calculated above. In the strain range AB (0.00556–0.01015) only the 90° plies crack and the 30° plies have linear response. Beyond point B, the 30° plies behave non-linearly but have no matrix cracks. Excellent agreement is observed for the Young's modulus but the Poisson's ratio prediction stops following the trend of the tests when the 30° plies start having non-linear behaviour. At that point, the non-linear behaviour of the 30° plies offsets decrease in Poisson's ratio caused by the cracks in the 90° plies and the prediction becomes almost horizontal. Predictions by Varna et al. are also shown in Fig. 14 showing higher accuracy than the present method for low strains but lower accuracy for higher strains.

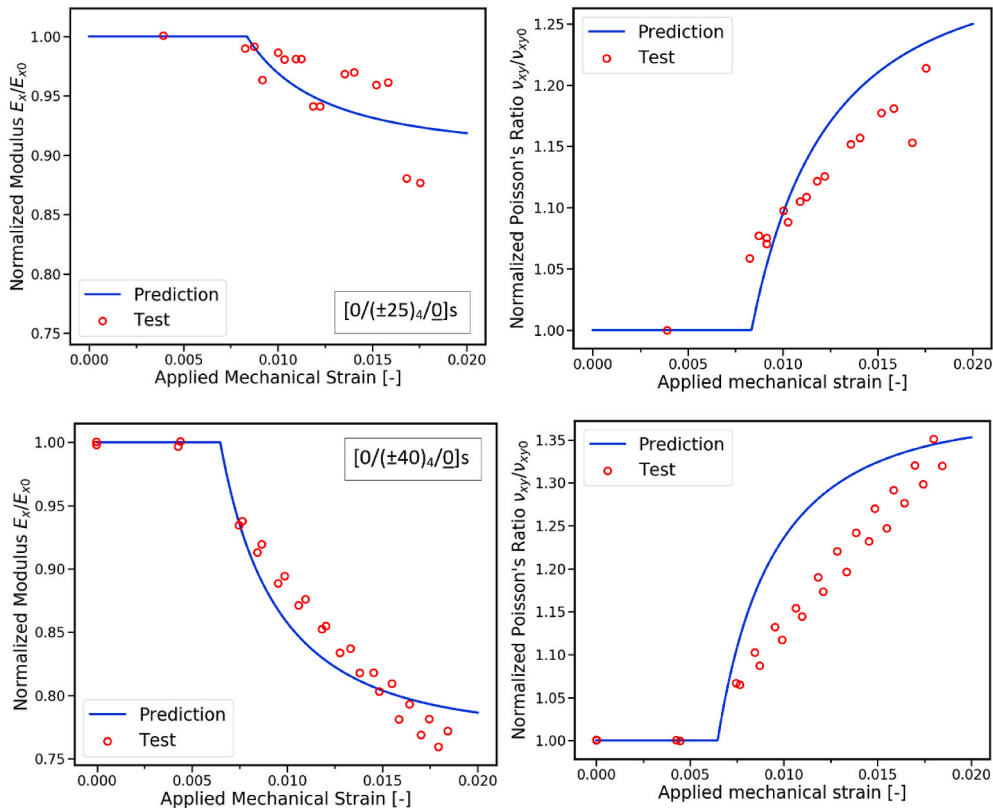


Fig. 16. Laminate stiffness predictions compared to test results from Ref. [9] for $[0/(\pm\theta)_4/0]_s$.

Further comparisons are shown in Figs. 15–16. The predictions by Varna et al. [10] are also shown in Fig. 15 showing less accuracy than the present method at higher strains. For the present method, there is excellent agreement in the Young's modulus. For the Poisson's ratio, the predictions capture the trends quite well. It is interesting to note that the predictions for the $[\pm 40/90_4]_s$ laminate show two kinks, one when the 40° plies become non-linear at an approximate applied axial strain of 0.0085 and one when matrix cracks appear in the 40° plies at an approximate applied strain of 0.0105. Even though there is scatter in the test data, it appears that these kinks, in particular the second one in the Poisson's ratio plot, capture the trend of the data with a sharp drop quite accurately.

Comparisons with several other laminates from Ref. [4,9,10], and [29] showed similar or better accuracy than that shown in Figs. 15 and 16, with one exception. The predictions for a $[0/(\pm 55)4/0]_s$ laminate did not match the test results from Ref. [9]. It is believed that the discrepancy may be due to some of the approximations made and the issue is under investigation.

3. Discussion and conclusions

The approach presented solves the local problem of matrix cracking in a ply under any combination of in-plane strains. It can determine the crack density and the local change in stiffness properties as a result of crack creation allowing a direct link between applied load and stiffness reduction. In addition, for cases containing shear loading, a bi-linear shear stress-strain approximation of the material shear stress-strain curve is combined with the stress solution to determine permanent shear strains in the ply as a function of strain level and crack spacing if cracks are present.

The method presented has several advantages: The stresses are obtained in closed form and the criterion for cracking based on average energy density is also in closed form. A minimum number of iterations may be needed when cracks or non-linearities cause load redistribution among plies and when checking for crack creations when shear strains are present. In a sense, the cracking criterion makes use of an average quantity that is analogous to the (average) energy release rate for the loading in question. A different criterion with experimentally measured critical energy release rate values can be used provided mode mixity is properly accounted for when different combinations of transverse and shear strain are applied. The proposed criterion accounts for different loading combinations by ensuring that the first cracks in a ply appear at the same time as a Hashin-type stress criterion would predict. Beyond first cracks, the stress criterion is no longer used.

The comparisons with published experimental data show good to excellent agreement for different materials and laminates. Being essentially in closed form, other than summing infinite series which converge rapidly, it can be used in progressive damage analysis to (almost) instantaneously update local stiffness at any location in a laminate under any in-plane loading. This eliminates the need for arbitrary assumption on stiffness knockdowns when cracks appear or use of models where damage variables must be estimated and/or inferred from additional tests. Furthermore, load redistribution between plies is accounted for as well as stacking sequence effects. This is done by updating the local strains in any ply by equations (44) and (45) which include any changes in the laminate compliance matrix a caused by crack creation and inelastic shear response. The efficiency and flexibility of the method makes it ideally suited for applications to fatigue analysis. Very good results obtained under fatigue loads will be presented in a future communication.

For a ply under transverse strain, the crack spacing and associated transverse stiffness change can be obtained through the creation of two master curves which are independent of material and surrounding layup (see Fig. 6). Thickness effects are accounted for by changing the in-situ transverse and/or shear strengths as necessary. In the laminate examples examined here, a factor of 8 change in thickness, from the 90° plies to

the 0 plies ($0 \neq 0$) in $[\pm 0/90_4]_s$ showed that the sensitivity to the in-situ strength values used, at least for this range of thicknesses, is rather small. Nevertheless, accurate knowledge of the transverse and shear in-situ strengths as a function of ply thickness and location in the layup, accounting for the relevant fracture phenomena, is necessary.

The method gives the crack-opening displacement for each matrix crack through exact calculation of the deflected shape of each crack surface formed. This suggests a definition of crack saturation as the point where the crack opening half way through the thickness of the ply equals half the crack spacing. Then, adjacent cracks touch each other and there is no more room for crack formation. However, calculations for typical materials showed that this is never reached. As crack density increases, the extra strain required to create the next crack increases rapidly leading to very high strains. At such strain levels other failure modes, including fiber failure in other plies will occur.

Results are load history-dependent. The crack creation history and the associated changes in ply stiffness will depend on the sequence with which strains are applied to a given ply. As cracks are created and/or a ply exhibits inelastic shear stresses, the strains through a laminate are redistributed leading to different cracking histories. For example, if a ply is under combined transverse and shear strains, applying each of them individually to obtain the final crack pattern and stiffness values will not give the same answer as proportionately increasing strains simultaneously.

By construction, the method presented predicts that the next crack will always be at the mid-point between cracks. While this is true for small crack spacings where the stresses reach their maximum value at the mid-point between cracks, it is not necessarily true for large crack spacings. Stresses reach their maximum values and remain constant over a portion of the region between cracks. Therefore, the next crack will appear at a random location within this region of uniform stresses and its creation depends on local defects the distribution of which is unknown. This means the crack spacing predicted by the method when cracks are far apart will be uniform and not necessarily accurate. This, however, does not affect the accuracy of the stiffness calculations.

Declaration of competing interest

The authors declare that they have no known competing financial interests or personal relationships that could have appeared to influence the work reported in this paper.

References

- [1] N. Laws, G. Dvorak, M. Hejazi, Stiffness changes in unidirectional composites caused by crack systems, *Mech. Mater.* 2 (2) (1983) 123–137.
- [2] M. Caslini, C. Zanotti, T. O'Brien, Study of matrix cracking and delamination in glass/epoxy laminates, *J. Compos. Technol. Res.* 9 (4) (1987) 121–130.
- [3] S.L. Ogin, P.A. Smith, P.W.R. Beaumont, Matrix cracking and stiffness reduction during the fatigue of a (0/90)_s GFRP laminate, *Compos. Sci. Technol.* 22 (1) (1985) 23–31.
- [4] A.L. Highsmith, K.L. Reifsnider, Stiffness-Reduction mechanisms in composite laminates, in: K.L. Reifsnider (Ed.), *Damage in Composite Materials*, ASTM STP 775, American Society for Testing and Materials, 1982, pp. 103–117.
- [5] G. Dvorak, N. Laws, M. Hejazi, Analysis of progressive matrix cracking in composite laminates I. Thermo elastic properties of a unidirectional composite with cracks, *J. Compos. Mater.* 19 (1985) 216–234.
- [6] Z. Hashin, Analysis of cracked laminates: a variational approach, *Mech. Mater.* 4 (1985) 121–136.
- [7] Z. Hashin, Analysis of orthogonally cracked laminates under tension, *J. Appl. Mech.* 54 (1987) 872–879.
- [8] R.J. Nuismer, S.C. Tan, Constitutive relations of a cracked composite lamina, *J. Compos. Mater.* 22 (1988) 306–321.
- [9] J. Varna, R. Joffe, N. Akshantala, R. Talreja, Damage in composite laminates with off-axis plies, *Compos. Sci. Technol.* 59 (1999) 2139–2147.
- [10] J. Varna, R. Joffe, R. Talreja, A synergistic damage-mechanics analysis of transverse cracking $[\pm 0/90_4]_s$ laminates, *Compos. Sci. Technol.* 61 (2001) 657–665.
- [11] R. Talreja, A synergistic damage mechanics approach to durability of composite material systems, in: *Progress in Durability Analysis of Composite Systems*, Brussels, 1996.

- [12] R. Talreja, A continuum mechanics characterization of damage in composite materials, in: *Proceedings of the Royal Society of London. Series A, Mathematical and Physical Sciences*, London, 1985.
- [13] R. Talreja, *Internal variable damage mechanics of composite materials*, in: *Yielding, Damage and Failure of Anisotropic Solids*, London, 1990.
- [14] W. Van Paepegem, I. De Baere, J. Degrieck, Modelling the nonlinear shear stress-strain response of glass fibre-reinforced composites. Part I: experimental results, *Compos. Sci. Technol.* 66 (2006) 1456–1478.
- [15] W. Van Paepegem, D.B. I, J. Degrieck, Modelling the nonlinear shear stress-strain response of glass fibre-reinforced composites. Part II: model development and finite element simulations, *Compos. Sci. Technol.* 66 (2006) 1465–1478.
- [16] H. Ahmadi, M. Hajikazemi, W. Van Paepegem, Closed-form formulae for prediction of homogenized ply-properties and laminate thermo-elastic constants in symmetric laminates containing ply cracks in multiple orientations, *Compos. Struct.* 241 (2020).
- [17] V. Singh, R. Talreja, Evolution of ply cracks in multidirectional composite laminates, *Int. J. Solid Struct.* 47 (2010) 1338–1349.
- [18] J. Varna, Modeling mechanical performance of damaged Laminates, *J. Compos. Mater.* 47 (20–21) (2013) 2443–2447.
- [19] C.V. Singh, R. Talreja, A synergistic damage mechanics approach to mechanical response of composite laminates with ply cracks, *J. Compos. Mater.* 47 (20–21) (2013) 2475–2501.
- [20] L.N. McCartney, Energy methods for modelling damage in laminates, *J. Compos. Mater.* 47 (20–21) (2013) 2613–2640.
- [21] M. Kashtalyan, C. Soutis, Modelling of stiffness degradation due to cracking in laminates subjected to multi-axial loading, *Phil. Trans. A* (2016) 374.
- [22] C. Kassapoglou, M. Kaminski, “Modeling damage and load redistribution in composites under tension–tension fatigue loading”, *Composites Part A* 42 (2011) 1783–1792.
- [23] Z. Hashin, Failure criteria for unidirectional fiber composites, *J. Appl. Mech.* 47 (1980) 329–334.
- [24] R. Joffe, A. Krasnikovs, J. Varna, COD-based simulation of transverse cracking and stiffness reduction in $[0/90_n]$ s laminates, *Compos. Sci. Technol.* 61 (5) (2001) 637–656.
- [25] J.T. Ryder, F.W. Crossman, A Study of Stiffness, Residual Strength and Fatigue Life Relationships for Composite Laminates, 172211, NASA CR, 1983. Tables 9 and 35.
- [26] J. Varna, L. Berglund, Multiple transverse cracking and stiffness reduction in cross-ply laminates, *J. Compos. Technol. Res.* 13 (1991) 99–106.
- [27] P.A. Lagacé, Nonlinear stress-strain behavior of graphite/epoxy laminates, in: *Proceedings of 25th Structures, Structural Dynamics and Materials Conference*, Palm Springs CA, 1984, pp. 63–73.
- [28] W. Van Paepegem, I. De Baere, J. Degrieck, Modelling the nonlinear shear stress-strain response of glass fibre-reinforced composites. Part II: model development and finite element simulations, *Compos. Sci. Technol.* 66 (2006) (2006) 1465–1478.
- [29] M.C. Lafarie-Frenot, F. Touchard, Comparative in-plane shear behaviour of long-carbon-fibre composites with thermoset or thermoplastic matrix, *Compos. Sci. Technol.* 52 (1994) 417–425.
- [30] P.D. Soden, M.J. Hinton, A.S. Kaddour, Lamina properties, lay-up configurations and loading conditions for a range of fibre-reinforced composite laminates, *Compos. Sci. Technol.* 58 (1998) 1011–1022.
- [31] Link. <https://docplayer.net/28421945-Apc-2-peek-thermoplastic-polymer.html>. (Accessed 13 July 2020).